Hindawi
Shock and Vibration
Volume 2023, Article ID 9600444, 14 pages
https://doi.org/10.1155/2023/9600444

Research Article

Monitoring of the Bond State between the Concrete-Filled Steel Tube Pile and Surrounding Soil

Daopei Zhu,[1] **Yali Hu**,[1] **and Cai Wu**[2,3]

[1]*School of Civil and Surveying & Mapping Engineering, Jiangxi University of Science and Technology, Ganzhou 341000, China*
[2]*School of Civil Engineering, Hubei Engineering University, Xiaogan 432000, China*
[3]*Changjiang River Scientific Research Institute, Changjiang Water Resources Commission, Wuhan 430010, China*

Correspondence should be addressed to Cai Wu; wucai@whut.edu.cn

Received 6 November 2022; Revised 28 April 2023; Accepted 3 May 2023; Published 18 May 2023

Academic Editor: P. Antonaci

The bonding state of the pile-soil interaction is complex. Traditional monitoring methods and tools have not been fully applied to monitor and evaluate it although it affects the lifecycle safety of the pile. In this study, a health monitoring method is proposed to evaluate the bonding state of the pile-soil contact area; it is a transient impact response method based on piezoelectric ceramic sensors to monitor the pile-soil bonding state. During the test, different damage degrees of the pile-soil bonding state were simulated by considering the working conditions of different soil densities and different crack depths as examples. A horizontal transient impact stress was applied to the pile top, and a piezoelectric ceramic sensor embedded in the pile detected the stress wave. As the stress wave response differs in different damage conditions, an energy index was established to quantitatively monitor the degree of damage.

1. Introduction

With the development of infrastructure in China, the pile foundation structure used in construction is often used in soft soil foundations. Pile foundations are mostly concealed deep underground. The safety and stability of the overall structure are related to the quality of the pile foundation; thus, safety monitoring of the pile foundation is critical. The overall state of the pile foundation can be determined and evaluated through monitoring. The pile-soil interaction mechanism is complex and changeable and has been studied extensively. Ai et al. [1] studied the interaction between layered saturated soft soil and pipe piles under static loading. Chen et al. [2] studied a calculation method based on the displacement pile-soil interaction and compared it with the traditional method. Huang et al. [3] studied the pile-soil interaction. Huang et al. [4] studied the influence of blasting load on the pile-soil structure interaction under dynamic loading. Gao et al. [5] studied the interaction between steel pipe piles and soil in river silt using an in situ test. In practice, test p-y (resistance-deflection) curves are a traditional tool to evaluate pile properties [6]. Low-strain and high-strain integrity tests have been used as traditional methods to evaluate the quality of pile foundations [7–9]. Although some progress has been made in recent research, with many factors affecting monitoring tools, the dynamic response of the pile must be determined considering the pile-soil interaction under a horizontal dynamic load to ensure the safety of the structure.

Structural health monitoring technology is an effective, economical, and real-time means of ensuring construction and service safety of engineering structures [10–12]. With the need to maintain infrastructure, only nondestructive testing can be used to monitor piles; thus, pile monitoring presents certain difficulties. Piezoelectric ceramic materials are used in actuators and sensors for their low cost, fast response, and solid actuation [13–14]. Jiang et al. used embedded piezoelectric ceramic sensors for monitoring [15–17]. In addition, an active sensing approach has been used in the health monitoring of concrete [18, 19], medical [20], and various civil infrastructures [21, 22], but not yet

enough research on pile-soil coupling monitoring and assessment has been obtained.

The test monitors the pile-soil bonding state through a transient impact method based on piezoelectric ceramic sensors. Different soil densities and crack depths were used in the test to study the pile-soil bond state; an energy index was used to evaluate the degree of damage. The transient impact at the top was monitored by the smart aggregate (SA) embedded in the soil. Combined with previous methods, this test uses a health monitoring method to evaluate the pile-soil bonding condition. The method has the characteristics of miniaturization, high sensitivity, and integration, increasing the reliability of pile-soil bonding evaluation. Experimental results verified the effectiveness of the proposed approach and inspired a new method for long-term monitoring of pile safety.

2. Methodology

2.1. Principle of Horizontal Impact Response of Pile-Soil Bonding Using the SA Sensor. A horizontal excitation signal was applied at the top of the sample test pile, and the SA sensor monitored the response, as shown in Figure 1. To ensure that the energy applied to the pile was the same, the hammer was suspended at the top of the pile and released from the same height each time. The test pile was a concrete-filled pile fixed with SA and placed in a steel tube for pouring. The SA was constructed using piezoelectric ceramic transducer (PZT) sheets, as shown in Figure 2. It reflects the coupling relationship between elastic (mechanical) properties and dielectric properties of piezoelectric materials. The quantity of the induced charge is proportional to the displacement of the PZT [23]. However, the sensor voltage recorded by the signal receiver has a positive relationship with the quantity of the electrical charge [24]. Therefore, it can be used to depict its mechanical stress by electric response data such as the wave signal response. To protect and waterproof the fragile PZT, epoxy resin was filled in the groove of the concrete block in producing the SA, as shown in Figure 3. The stability of the concrete-filled steel tubular piles with SA sensors embedded in the soil was ensured. The principle is that when the PZT piece becomes larger from the soil-binding force, the sensor response signal becomes weaker. The bond state between the pile and soil can be evaluated through the strength of the response signal.

In this work, a transient impact-sensing method based on piezoelectric ceramics was used to monitor the bond state between the pile and soil. The principle is that when the PZT piece becomes larger from the soil-binding force, the sensor response signal becomes weaker. The bond state between the pile and soil can be evaluated through the strength of the response signal.

For the same type of soil, the mechanical properties change with the soil density because the density determines its stiffness. Soil density was measured using the ring cutter method. The method is described as follows: First, the ring cutter is wiped clean, and the mass and volume of the ring cutter are measured. Cohesive soil is measured using an artificial soil sampler, and the soil samples are cut. The edge

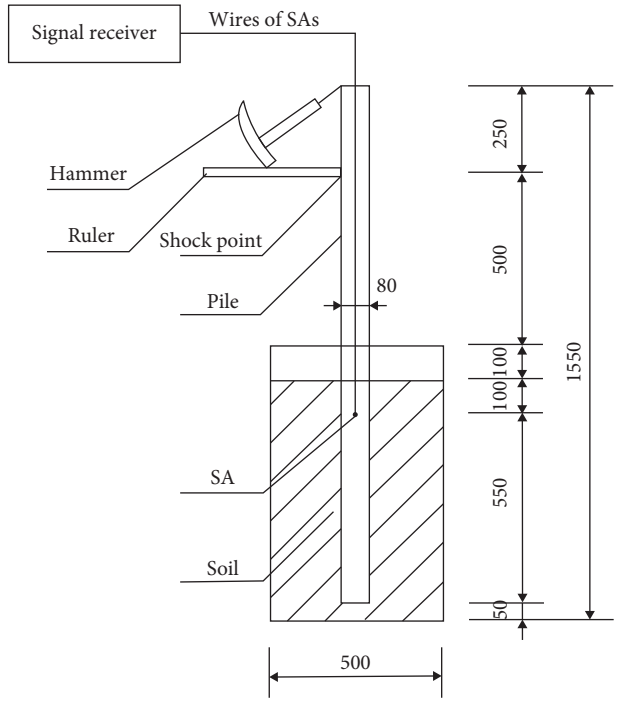

Figure 1: Schematic of the test device (unit: mm).

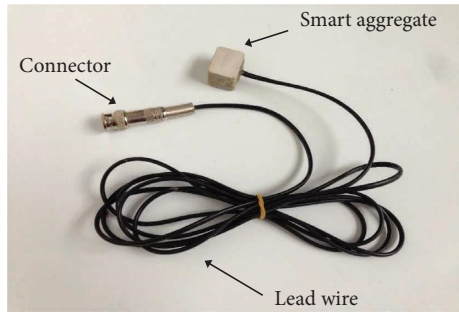

Figure 2: Smart aggregate connected to the BNC connector.

of the ring cutter is placed on the soil sample and pressed vertically. The mass of the soil is obtained by subtracting the mass of the ring cutter after weighing with a balance; the soil density is obtained using the volume of the ring cutter. Different soil densities around the pile provide different boundary conditions. Similarly, crack damage between the pile and soil provides different boundary conditions. In order to simulate the crack damage, the ring cutter method was used to take the soil. The method is described as follows: First, the ruler is used to measure 2 cm to determine the position 2 cm away from the concrete-filled steel tube pile. The ruler is used to measure and determine the position 5 cm, 10 cm, and 15 cm away from the bottom of the ring cutter. The blade of the ring cutter is pressed into the soil vertically and steadily with the same force until the sample in the ring cutter reaches the specified height. The soil around the ring cutter is cut with the soil cutter, the ring cutter is taken out, the excess soil at both ends of the ring cutter is carefully cut off, and the soil outside the ring cutter is wiped

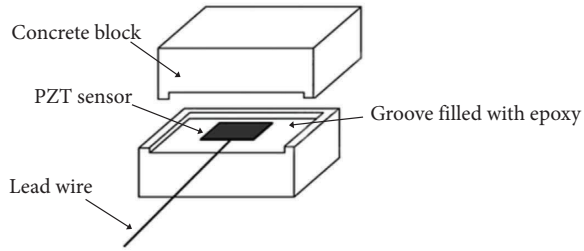

Figure 3: Internal structure of the smart aggregate.

off. The crack was located on the pile-soil interface, as shown in Figure 4. Changes in the boundary conditions of soils with different densities and crack depths lead to different responses of the SA to stress waves. The greater the binding force on the SA, the weaker the received response signal. Thus, the bond state between the pile and the soil can be determined from the response signal.

2.2. Signal Analysis Method. In this work, the time-domain analysis method was used to study the relationship between the SA response signal and pile-soil bonding state. The signal value was calculated to reflect the degree of bonding between the pile and soil. In time-domain analysis, the statistical eigenvalues include the maximum, minimum, mean, mean square, and variance of the signal amplitude and the energy and power of the signal, of which the energy of the signal is more commonly used. The signal energy index E is calculated as

$$X_i = (x_{i1}, x_{i2}, ..., x_{im}), \tag{1}$$

where X_i is a set of discrete data for the signal measured by the sensor at $[ii]$, x_{ij} is the sensor voltage at the j^{th} sampling point at $[ii]$, and m is the number of sample points for each sampling duration.

E_i is an indicator of the degree of bonding of piles to soil, which is defined as

$$\begin{aligned} E_i &= \|X_i\|^2 \\ &= x_{i1}^2 + x_{i2}^2 + ... + x_{im}^2 \\ &= \sum_{j=1}^{m} x_{ij}^2 \quad (i = 1, 2, ...). \end{aligned} \tag{2}$$

The wave transmission energy measured by the energy index can determine the degree of bonding between the soil and pile. When the density of the soil is low, the bonding force between the soil and pile is small. After a horizontal stress is applied using the hammer, the energy dissipates minimally into the soil, and the energy obtained by the SA response is large. With an increase in crack damage depth, the horizontal force of the pile-soil boundary constraint becomes increasingly weaker; thus, the wave signal at greater depths is less dispersed into the soil, and the SA test wave signal is stronger. Analysis of the signal wave response can indicate the pile-soil bonding condition. At high temperatures, the sensor-coating material melts, solder joints open, and the stress of the elastomer changes; thus, the test environment should be maintained at room temperature (20°C) to reduce the error caused by temperature.

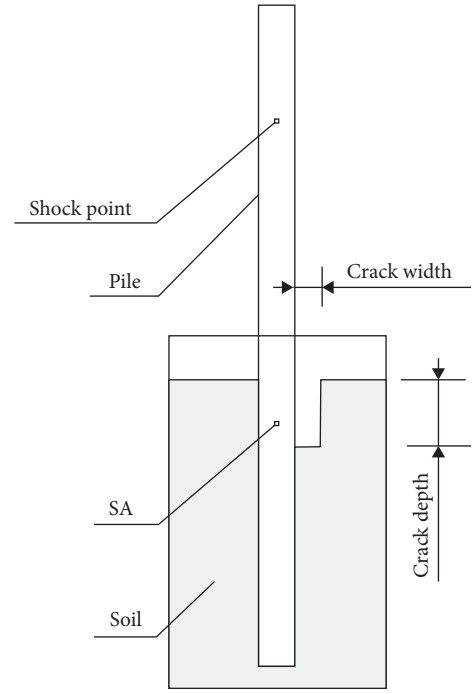

Figure 4: Location of crack damage.

3. Experimental Investigation

3.1. Experimental Setup. Lead zirconate titanate (PZT) is a commonly used piezoelectric material with dimensions of 10 mm × 10 mm × 0.3 mm. It exhibits both piezoelectric and inverse piezoelectric effects. A charge (piezoelectric effect) is generated when it is subjected to external stress. Strain occurs when an external electric field is applied (inverse piezoelectric effects). As the PZT-5H-type ceramic in PZT has a high sensitivity and good time stability, the PZT-5H-type ceramic was used as the sensor in this experiment. A test box with dimensions of 500 mm (length) × 400 mm (width) × 800 mm (height) was prepared in advance and filled with test soil. A concrete-filled steel tube pile with a length of 1500 mm, a width of 80 mm, and a thickness of 60 mm was embedded in the soil, as shown in Figure 5. The particle size of the selected test soil was between 0.005 mm and 0.05 mm, with high plasticity and low permeability, as shown in Figure 6. The steel tube was composed of two-channel steels. The SA sensor with a PZT sheet was placed in a steel tube and poured with concrete. The concrete strength grade was C30, with an elastic modulus of $E_0 = 3 \times 10^{10}$ Pa and Poisson's ratio of $\nu = 0.2$. The position of the SA sensor in the concrete-filled steel tube pile is shown in Figure 3; it is embedded 10 cm from the soil surface. As shown in Figure 7, a horizontal transient impact was generated by hammering; the position of the controlled impact was obtained using a ruler attached to the surface of the steel tube placed 25 cm from the top of the test pile. When horizontal vibration was

applied to the steel pipe, the SA sensor received different signals because of different soil densities and crack depths being used to measure the difference in the bonding force between the steel pipe and the soil. In this test, the degree of bonding between the pile and soil was studied using six test examples.

3.2. Testing Procedure. Three types of soils with different densities were used in the experiment. The soil particle size was between 0.005 mm and 0.05 mm, and the water content was the same. As the compactness of the soil is related to the soil density, by tamping the soil and increasing its density, the degree of bonding between the pile and soil can be improved. To better constrain the bonding of the pile and soil, the selected soil densities were 1151 $kg{\cdot}m^{-3}$, 1324 $kg{\cdot}m^{-3}$, and 1406 $kg{\cdot}m^{-3}$. The experiment was divided into A and B groups. A horizontal excitation signal was applied to the top surface of the pile using a hammer. To ensure the accuracy of the test data, the hammer was controlled to be released from the same height using the installed ruler, ensuring the same initial horizontal transient impact energy, as shown in Figure 7. When the hammer hit the pile, the SA sensor responded to the impact; the response change reflected the degree of bonding between the soil and piles. The SA sensor response signal was recorded using the signal receiver, as shown in Figure 5.

In Group A, the soil densities were 1151 $kg{\cdot}m^{-3}$, 1324 $kg{\cdot}m^{-3}$, and 1406 $kg{\cdot}m^{-3}$, respectively, as shown in Figure 8. In Group B, the crack damage width of the pile was 2 cm, the soil density was 1436 $kg{\cdot}m^{-3}$, the thickness of the cracking damage was 8 cm, and the depth of the cracking damage was 5 cm, 10 cm, and 15 cm, as shown in Figure 9.

3.3. Results and Analyses. The time-domain signal of the Group A SA sensor is shown in Figure 10. It is observed that the signal response of the SA sensor is different in different density conditions. With a soil density of 1151 $kg{\cdot}m^{-3}$, the maximum response signal is 3912.54 mV; with a soil density of 1324 $kg{\cdot}m^{-3}$, the maximum response signal is 3196.11 mV; with a soil density of 1406 $kg{\cdot}m^{-3}$, the maximum response signal is 2647.92 mV. It can be concluded that when the soil density on the PZT patch was large, the deformation of the SA sensor was small, the response signal was weak, and duration was short. In contrast, when the soil density was low, the sensor signal was strong and lasted longer. The amplitude of the signal decreased with an increase in the soil density. Thus, with the constraints of a certain damage depth and damage range, greater soil density produces better compactness, providing better pile-soil bonding. Owing to different degrees of damage, Groups A and B received different SA sensing signals. The SA sensing signal for Group B is shown in Figure 11. When the damage crack depth was 5 cm, the maximum response signal was 1893.12 mV; when the damage crack depth was 10 cm, the maximum response signal was 2580.44 mV; when the damage crack depth was 15 cm, the maximum response signal was 3520.57 mV. As the crack depth gradually increased, the soil constraint on the SA gradually decreased, and more signals were received by the SA. The signal amplitude increased with the increasing fracture damage depth.

The severity of pile-soil bonding can also be expressed by the energy index. To intuitively reflect the attenuation of the stress wave energy, the energy indexes of all tests were calculated using equations (1) and (2). The energy indexes for different soil density damages are shown in Figure 12. The energy indexes for different crack-damage depths are shown in Figure 13. In the Group A test, the signal amplitude recorded by the SA sensor decreased with the increasing soil density, indicating that after the horizontal transient impact, the PZT patch vibrated along the thickness direction [25] and the stress wave passed through the PZT patch and propagated to the soil. As the soil had high density, good compactness, few voids, and good transmission performance, and duration was short, a small amount of energy was retained on the PZT patch, as shown in Figure 12. In Group B, the energy increased with the increasing crack failure depth. The cohesive force of the soil pile decreased due to pile damage and crack damage. The energy transferred by the soil decreased, and the residual energy on the PZT patch increased, as shown in Figure 13. The time-domain analysis method has wide application prospects in estimating the bond relationship between piles and soil. It can provide damage warnings and evaluate the bond degree between the pile and soil in real time. The test data show that the constraints on the PZT patches were different due to different soil densities; thus, the signal response of SA sensors along the pile was different with different constraint depths. If multiple SA sensors are placed in soils of different densities and depths, the health status of a structure can be monitored more accurately and continuously. However, there are still some problems; for example, the impact of different ambient temperatures, the influence of different crack ranges, the contact area between the pile and soil, and the influence of multiple pile cracks should be considered in future research.

4. Numerical Verification

To verify the accuracy of the test results and further analysis the influence of the soil density and crack depth on pile-soil bonding, a finite element calculation model was established using ABAQUS software. The model was divided into two parts: the soil and pile, as shown in Figure 14. The model considered the pile as an elastic material and the soil as a Mohr Coulomb material. The clay model was 50 cm long, 40 cm wide, and 80 cm high. The pile was 8 cm long, 6 cm wide, and 150 cm high. The elastic modulus, Poisson's ratio, friction angle, and dilatancy angle of the soil were 30 MPa, 0.3, 30 degrees, and 0 degrees, respectively. The elastic modulus, Poisson's ratio, and density of the square steel tube were 206 GPa, 0.2, and 7890 $kg{\cdot}m^{-3}$, respectively. A 200 N coupling force was applied at a distance of 25 cm from the concrete-filled steel tube pile. The surrounding soil was completely fixed with the bottom. C30 concrete was used in the square steel tube, and the soil and piles were connected by binding to directly reflect the stress of different soil densities and crack depths after instantaneous horizontal impact.

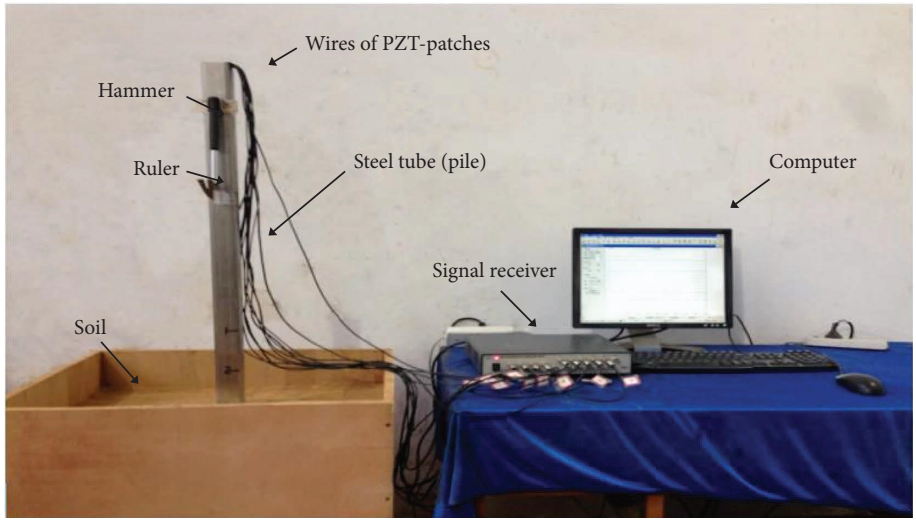

Figure 5: Transient impact response test system.

Figure 6: Test soil.

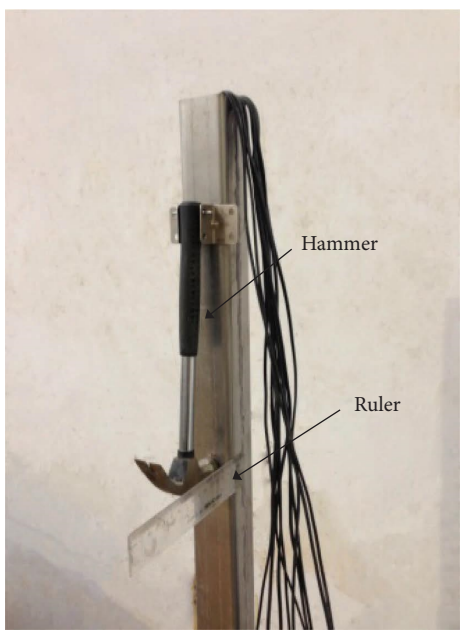

Figure 7: Instantaneous horizontal impact with a hammer and measurement of compaction with a ruler.

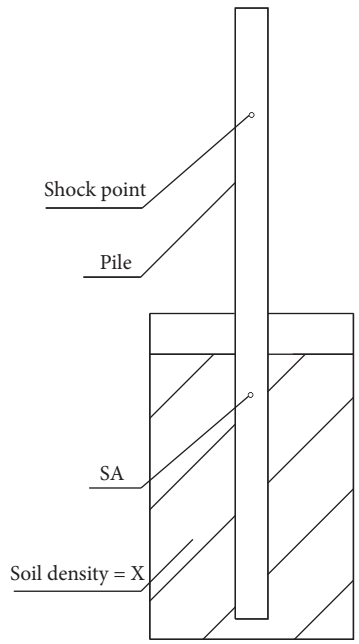

Group	A		
Instance	1	2	3
Temperature (°C)	20	20	20
The value of X (kg·m^{-3})	1151	1324	1406

Figure 8: Different soil densities (unit: kg·m^{-3}).

Three finite element models were established. The soil densities were 1151 kg·m^{-3}, 1324 kg·m^{-3}, and 1406 kg·m^{-3}. The normal stress distribution of the square steel pipe was different with different soil densities, as shown in Figure 15. When the soil density was 1151 kg·m^{-3}, the maximum stress was 1.422 MPa; when the soil density was 1324 kg·m^{-3}, the maximum stress was 1.402 MPa; when the soil density was 1406 kg·m^{-3}, the maximum stress was 1.377 MPa. It is observed that with the same external force, the maximum stress value of the square steel pipe decreased with an increase in the soil density. The principle is that when the density of the soil increases, the gap between the soil particles becomes smaller, the particles are in close contact, and the occlusion between the particles increases, friction resistance increases, so the cohesion of the soil increases, and the shear strength of the soil increases. Therefore, the maximum strain force of the pile becomes smaller, and the bearing capacity becomes larger. It can be seen in Figures 10 and 15 that the amplitude of the signal is closely related to the maximum stress value of the square steel tube.

Then, three more finite element models were established. The width of the peeling damage was 2 cm; the damage depths were 5 cm, 10 cm, and 15 cm, as shown in Figure 16. Figures 17(a)–17(c) show three damage states with a cracking damage thickness of 6 cm and a soil density of 1436 kg·m^{-3}. The stress distribution was observed in different damage depth conditions after instantaneous horizontal force. The maximum stress was 163.9 kPa with a damage depth of 5 cm; the maximum stress was 247.8 kPa with a damage depth of 10 cm; the maximum stress was 314.5 kPa with a damage depth of 15 cm. With instantaneous horizontal action, the stress of the square steel pipe increased with an increase in the damage depth with the same horizontal load. The principle is that when the depth of crack damage increases, the cohesive force between the soil and pile decreases and the interaction between the pile and soil decreases. The stress wave cannot propagate through the crack, so the stress wave left in the pile increases, and the corresponding stress value becomes larger. The stress value changes with the change in the crack depth. It can be seen in Figures 11 and 17 that the amplitude of the signal has a close relationship with the stress distribution of the square steel tube.

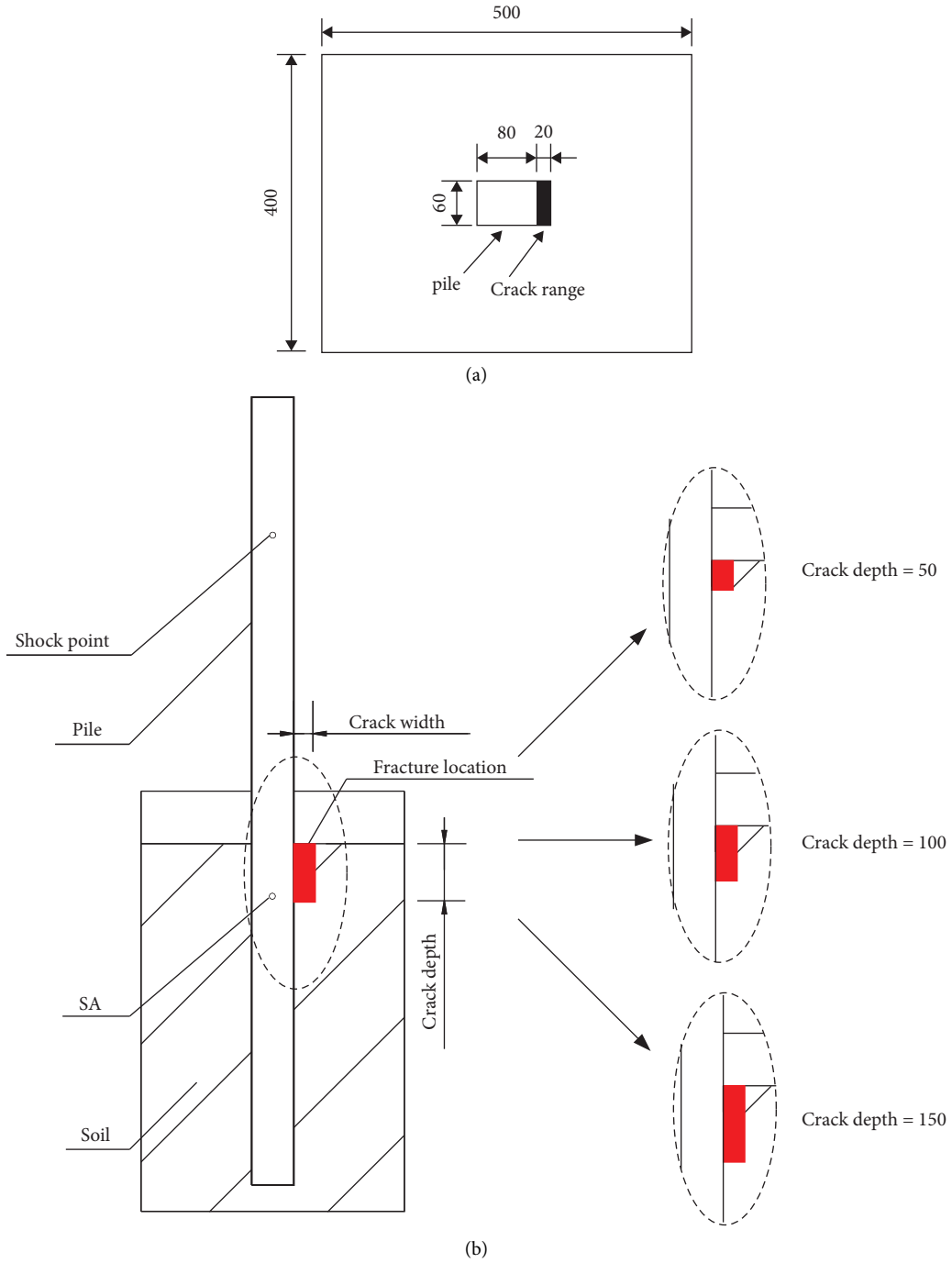

Figure 9: Different fracture damage depths (unit: mm): top (a) and front (b) views of the model.

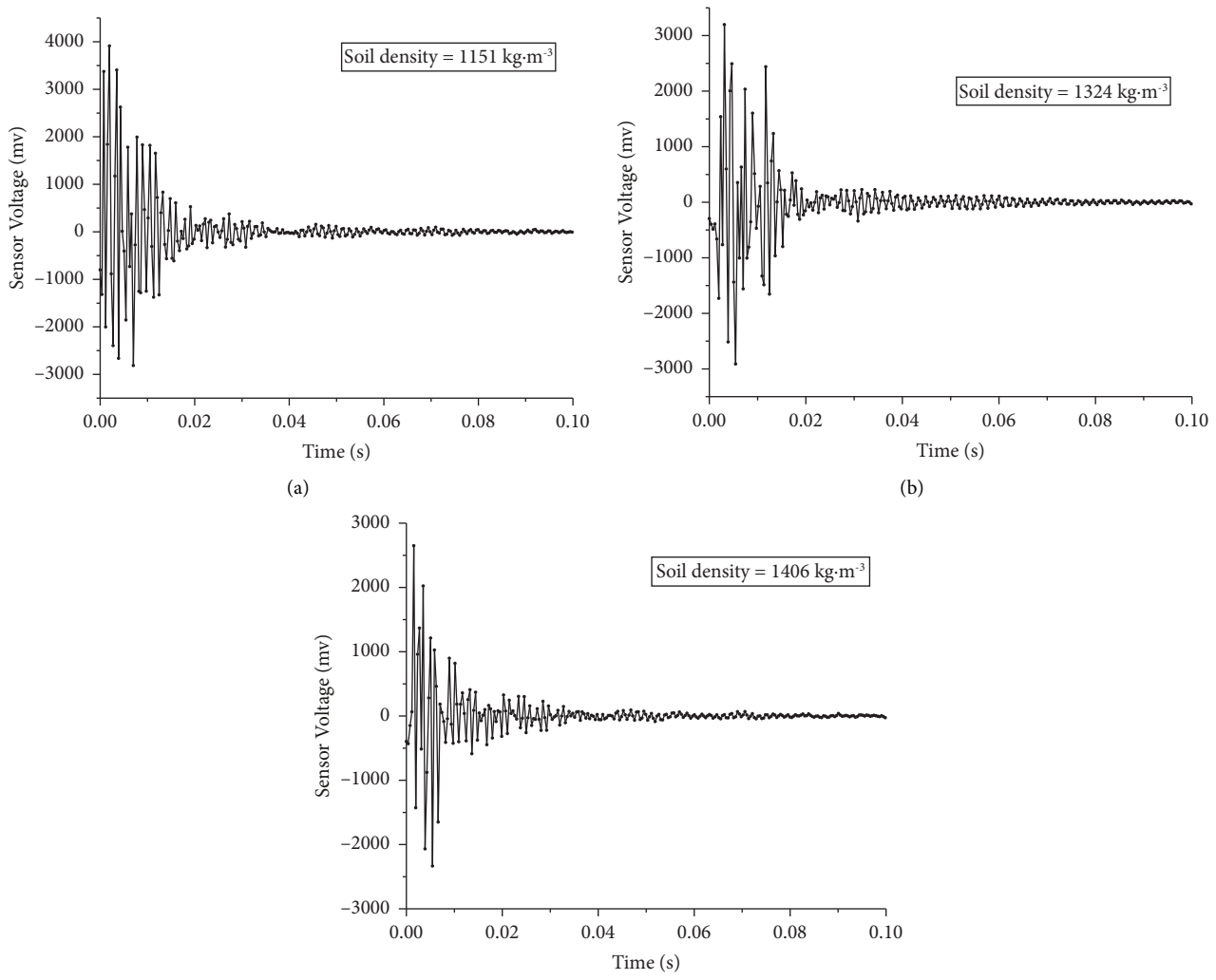

Figure 10: SA signals in soils with different densities: (a) soil density = 1151 kg·m^{-3}; (b) soil density = 1324 kg·m^{-3}; (c) soil density = 1406 kg·m^{-3}.

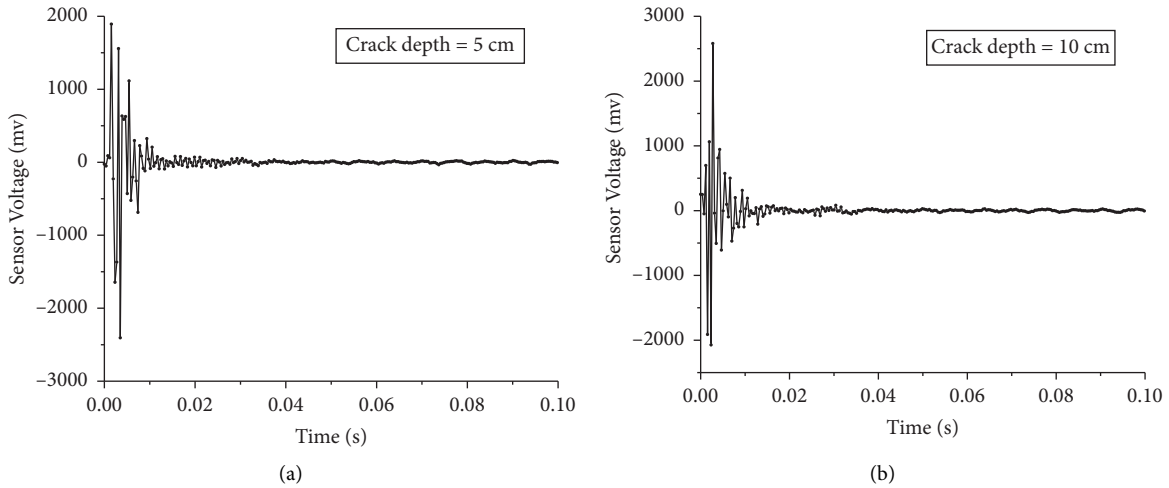

Figure 11: Continued.

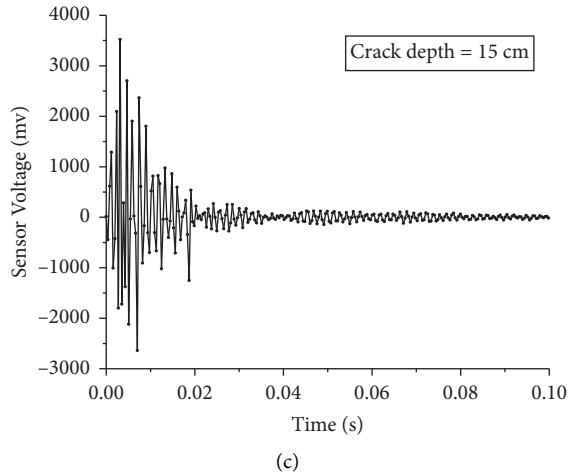

(c)

Figure 11: SA signals in soils with different fracture damage depths: (a) crack depth = 5 cm; (b) crack depth = 10 cm; (c) crack depth = 15 cm.

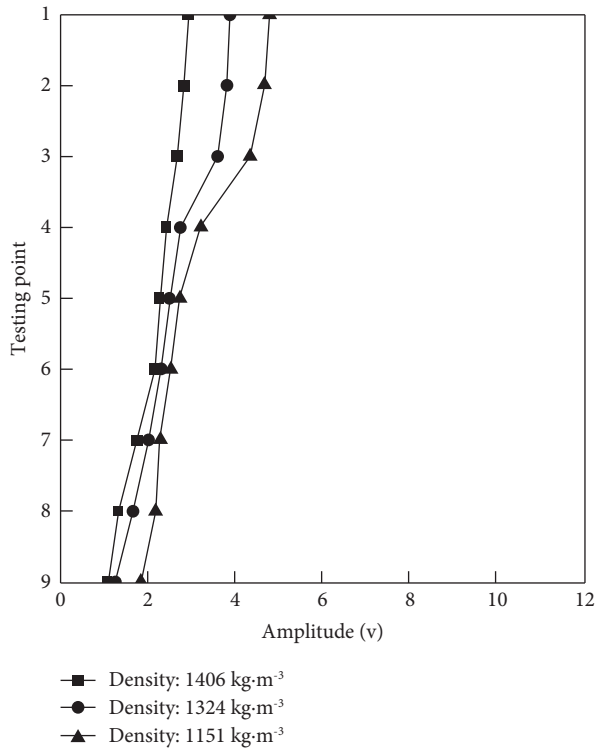

Figure 12: Energy indicators of density damage in different soils.

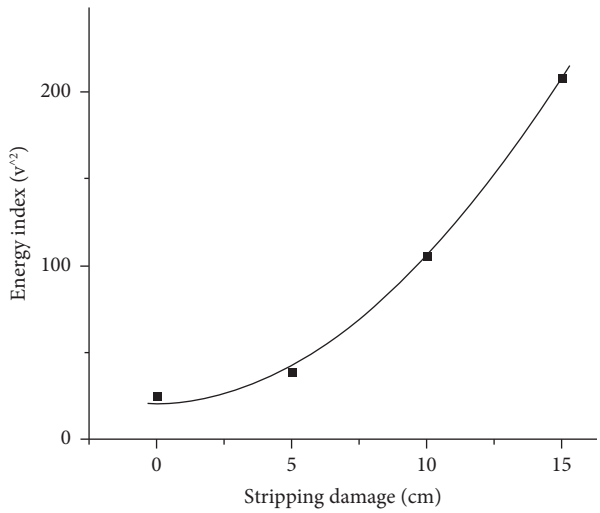

Figure 13: Energy indicators for different fracture damage depths.

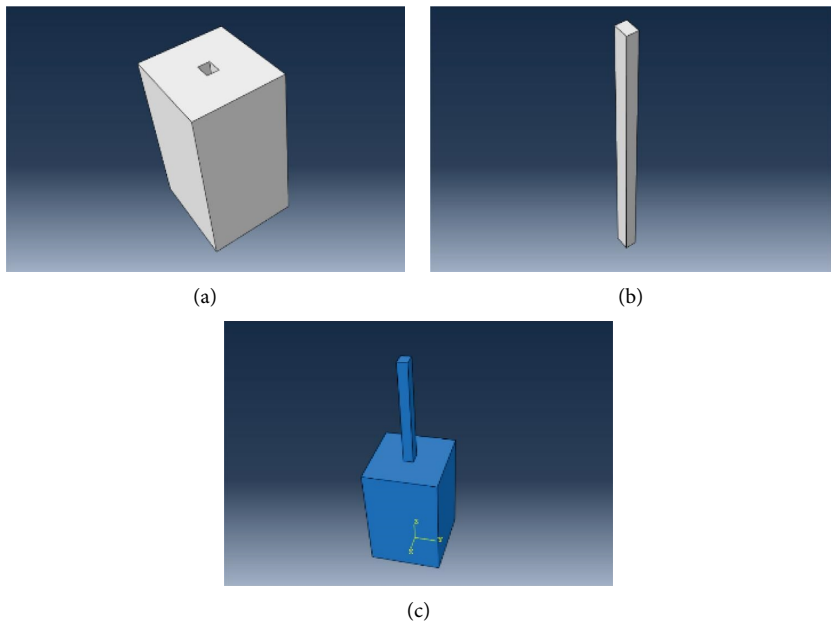

Figure 14: Schematic of pile and soil mass.

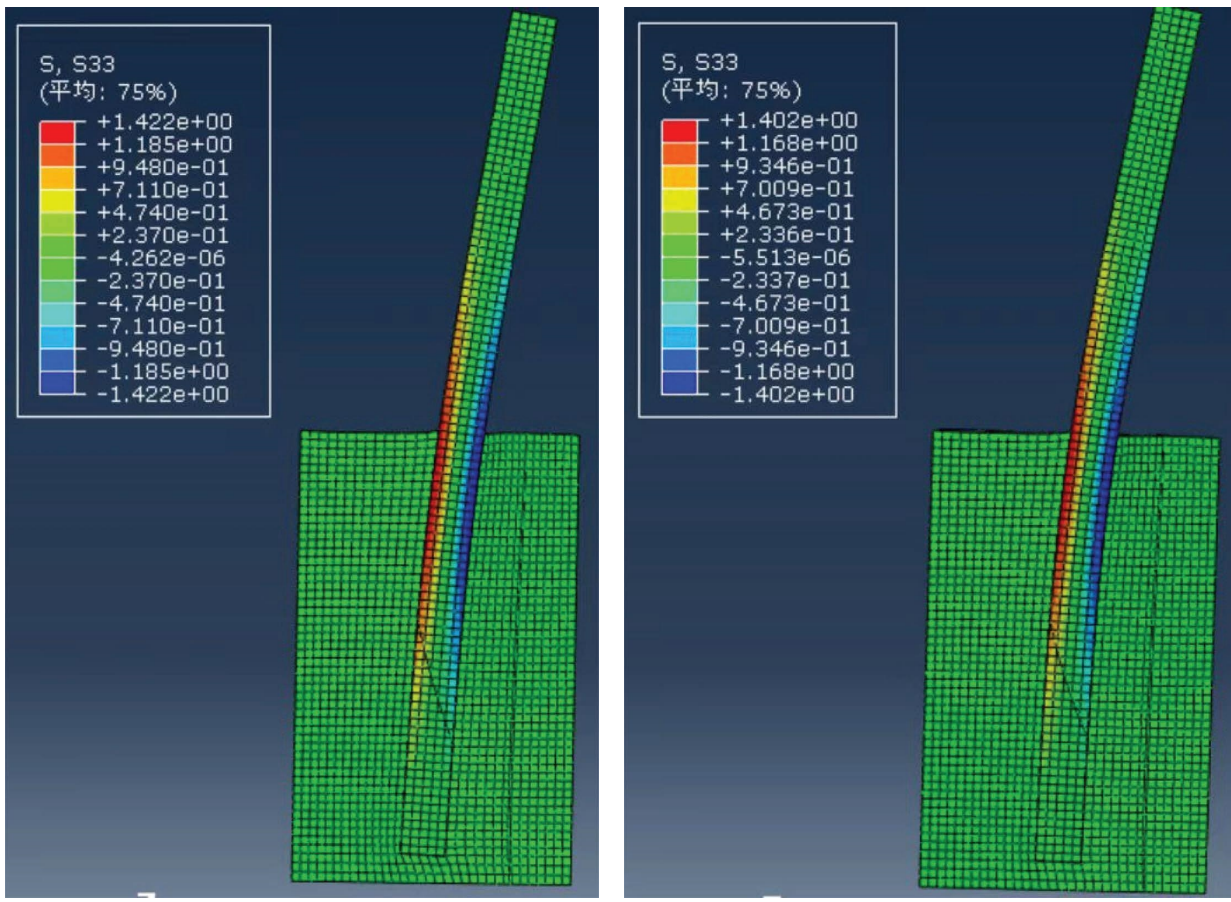

(a) (b)

Figure 15: Continued.

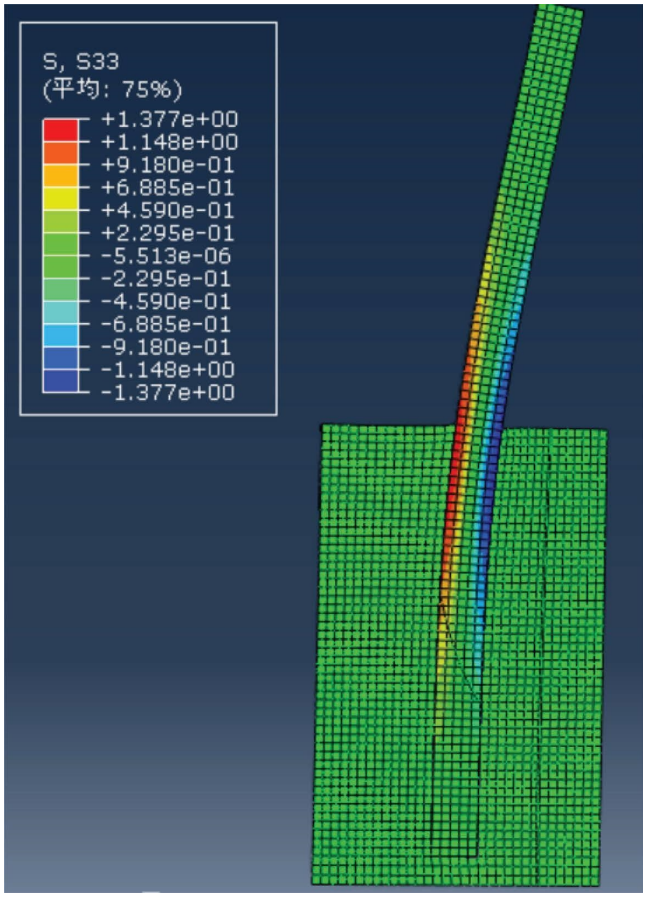

(c)

Figure 15: Normal stress result diagram for the square steel pipe and soil: damage state with a soil density of (a) 1151 kg·m^{-3}; (b) 1324 kg·m^{-3}; and (c) 1406 kg·m^{-3}.

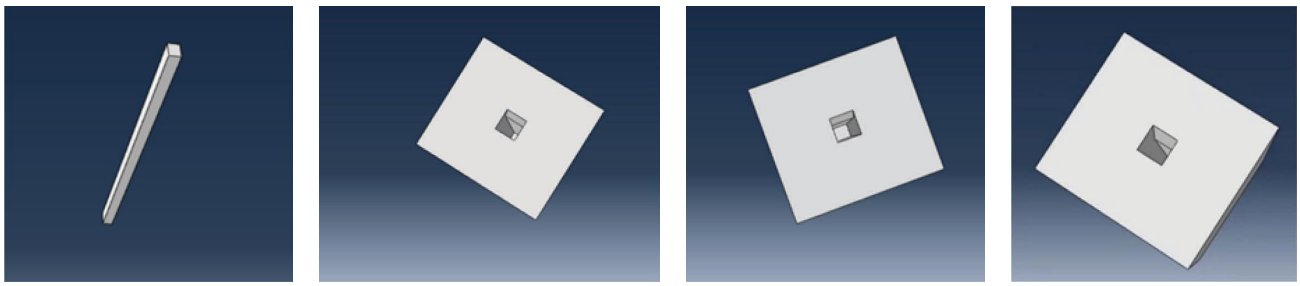

(a) (b) (c) (d)

Figure 16: Crack damage model: (a) model piles; (b) depth of injury is 5 cm; (c) depth of injury is 10 cm; (d) depth of injury is 15 cm.

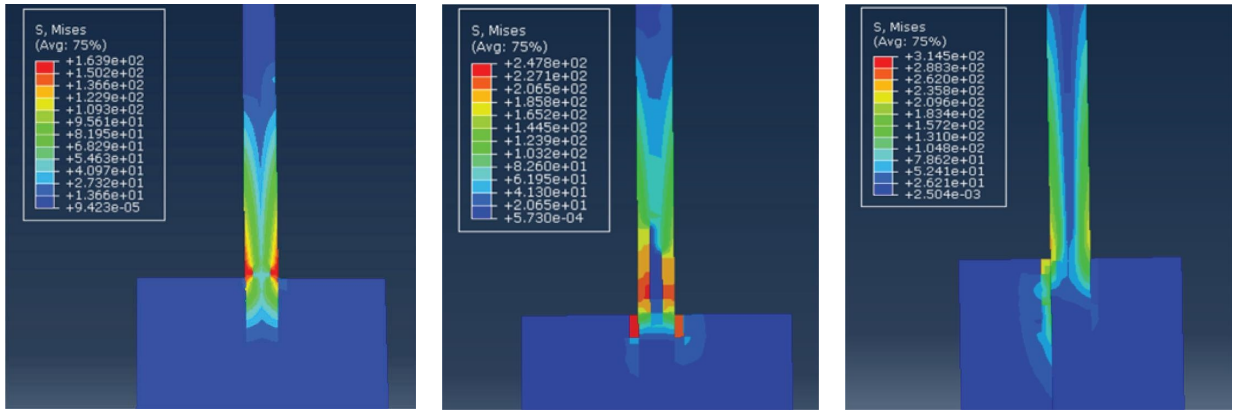

(a) (b) (c)

Figure 17: Stress result diagram (unit: MPa):injury with a depth of (a) 5 cm, (b) 10 cm, and (c) 15 cm.

5. Conclusion

To explore the pile-soil bonding state, this study proposed a transient impact response method based on an SA sensor. Two typical working conditions were studied by varying the soil density and crack depth. The signal waves varied with changes in the soil density and crack depth.

(1) The influence of the soil density on the sensor signal was studied by varying the soil density. It can be concluded that as the soil density increases, there is a strong constraint on the pile soil, the SA sensor signal weakens, and the amplitude decreases.

(2) The effect of the crack depth on the sensor signal was studied by varying the crack depth. It can be concluded that as the crack depth increases, the adhesion of the soil pile decreases, the SA sensor signal becomes stronger, and the amplitude increases.

(3) Comparison of the energy indicators simulated by the model using the structural data of the healthy state can be used to quantitatively assess the degree of damage to a structure, hh2such as slip or shedding, indirectly leading to a direct estimate of whether the pile and soil are effectively combined. This study monitors the entire construction process, monitors the defects of the pile body, determines the integrity category of the pile body, and is used to predict whether the future structure will be damaged and provide early warning.

Data Availability

The experimental data used to support the findings of this study are included within the article.

Conflicts of Interest

The authors declare that there are no conflicts of interest regarding the publication of this paper.

Acknowledgments

The authors acknowledge the financial support from the Central Non-Profit Scientific Research Fund for Institutes of China (No. CKSF2021431/CL), the Natural Science Foundation of Xiaogan, China (No. XGKJ2021010015), and the National Natural Science Foundation of China (No. 52179122).

References

[1] Z. Y. Ai, H. Wang, and W. J. liu, "Quasi-static interaction between pipe piles and multilayered saturated soft soils with a fractional viscoelastic model," *Acta Geotechnica*, vol. 16, no. 1, pp. 317–333, 2021.

[2] B. C. Chen, X. Y. Luo, F. Y. Huang, R. Dong, and J. Xue, "Displacement-based simplified calculation for pile-soil interaction under reciprocating low-cycle pseudo-static loads," *Journal of Testing and Evaluation*, vol. 49, no. 4, Article ID 20180742, 2021.

[3] F. Y. Huang, Y. L. Shan, G. D. Chen, Y. Lin, H. Tabatabai, and B. Briseghella, "Experiment on interaction of abutment, steel H-pile and soil in integral abutment jointless bridges (IAJBs) under low-cycle pseudo-static displacement loads," *Applied Sciences*, vol. 10, no. 4, p. 1358, 2020.

[4] B. Huang, Q. C. Gao, J. G. Wang et al., "Dynamic analysis of pile-soil-structure interaction system under blasting load," *Applied Mechanics and Materials*, vol. 638–640, pp. 433–436, 2014.

[5] M. Gao, D. B. Chin, M. Y. Ma, and R. G. Sun, "A study of pile-soil interaction behavior under static, cyclic and dynamic lateral loadings," *Journal of Energy Resources Technology*, vol. 106, no. 4, pp. 496–501, 1984.

[6] A. F. Hu, B. W. Nan, and Y. Chen, "Modified p-y curves method based on degradation stiffness model of sand," *Journal of Shanghai Jiaotong University*, vol. 54, no. 12, pp. 1316–1323, 2020.

[7] Y. P. Zhang, M. H. El Naggar, W. Wu, and Z. Wang, "Torsional low-strain test for nondestructive integrity examination of existing high-pile foundation," *Sensors*, vol. 22, no. 14, p. 5330, 2022.

[8] A. G. Davis, "The nondestructive impulse response test in north America: 1985-2001," *NDT & E International*, vol. 36, no. 4, pp. 185–193, 2003.

[9] Z. L. Li and H. Y. Gao, "The comprehensive application of high-low strain test in detecting pile foundations," *Applied Mechanics and Materials*, vol. 170–173, pp. 191–194, 2012.

[10] K. Y. Wong, "Design of a structural health monitoring system for long-span bridges," *Structure and Infrastructure Engineering*, vol. 3, no. 2, pp. 169–185, 2007.

[11] P. J. Lefebvre, *The Instrumentation, Testing, and Structural Modeling of a Steel Girder Bridge for Long-Term Structural Health Monitoring*, University of New Hampshire, Durham, NH, USA, 2010.

[12] D. P. Zhu, S. Y. Tian, H. C. Yan, and Z. L. Wang, "A feasibility study on monitoring pile-soil bonding condition using piezoceramic transducer and horizontal impact," *Journal of Sensors*, vol. 2021, Article ID 5575854, 11 pages, 2021.

[13] A. C. Rutherford, G. Park, and C. R. Farrar, "Non-linear feature identifications based on self-sensing impedance measurements for structural health assessment," *Mechanical Systems and Signal Processing*, vol. 21, no. 1, pp. 322–333, 2007.

[14] S. Ritdumrongkul, M. Abe, Y. Fujino, and T. Miyashita, "Quantitative health monitoring of bolted joints using a piezoceramic actuator-sensor," *Smart Materials and Structures*, vol. 13, no. 1, pp. 20–29, 2004.

[15] T. Jiang, Q. Kong, Z. Peng et al., "Monitoring of corrosion-induced degradation in prestressed concrete structure using embedded piezoceramic-based transducers," *IEEE Sensors Journal*, vol. 17, no. 18, pp. 5823–5830, 2017.

[16] H. J. Zhou, Y. Q. Liu, Y. Y. Lu et al., "In-situ crack propagation monitoring in mortar embedded with cement-based piezoelectric ceramic sensors," *Construction and Building Materials*, vol. 126, no. 1, pp. 361–368, 2016.

[17] K. Xu, Q. Z. Kong, S. Chen, and G. Song, "Early determination of the presence of low strength concrete in reinforced concrete beam-column joints using piezoceramic-based transducers," *IEEE Sensors Journal*, vol. 17, no. 11, pp. 3244–3250, 2017.

[18] J. L. Lu, S. M. Hu, W. Li et al., "A biodegradable and recyclable piezoelectric sensor based on a molecular ferroelectric embedded in a bacterial cellulose hydrogel," *ACS Nano*, vol. 16, no. 3, pp. 3744–3755, 2022.

[19] X. M. Yang and Z. J. Li, "Application of cement-based piezoelectric sensing system to concrete structure," *Earthquake Engineering and Engineering Vibration*, vol. 32, no. 5, pp. 111–118, 2012.

[20] L. Qin, E. R. Wang, Q. Qin, T. Yang, and F. Gao, "Monitoring of dynamic strain response in concrete structure based on piezoelectric sensors," *The Open Civil Engineering Journal*, vol. 11, no. 1, pp. 992–1002, 2017.

[21] F. Y. Sun, W. Zhao, and N. Fan, "Design of smart aggregates: towards rapid clinical diagnosis of hyperlipidemia in human blood," *Advanced Materials*, vol. 34, Article ID e2207671, 2022.

[22] A. Laskar, H. C. Gu, Y. L. Mo, and G. Song, "Progressive collapse of a two-story reinforced concrete frame with embedded smart aggregates," *Smart Materials and Structures*, vol. 18, no. 7, Article ID 075001, 2009.

[23] J. L. Zhao, T. F. Bao, S. Chen, and T. Kundu, "Smart aggregate-piezoceramic patch combination for health monitoring of concrete structures," *Journal of Sensors*, vol. 2016, no. 1, 7 pages, Article ID 3270916, 2016.

[24] S. H. Choy, X. P. Jiang, K. W. Kwok, and H. Chan, "Piezoelectric and dielectric characteristics of lead-free BNKLBT ceramic thick film and multilayered piezoelectric actuators," *Ceramics International*, vol. 36, no. 8, pp. 2345–2350, 2010.

[25] S. Hou, H. B. Zhang, and J. P. Ou, "Stone-based smart aggregates using PZT for compressive seismic stress monitoring," in *Proceedings of the 15th World Conference on Earthquake Engineering*, pp. 1–10, Lisbon, Portugal, September 2012.

[26] C. V. Newcomb and I. Flinn, "Improving the linearity of piezoelectric ceramic actuators," *Electronics Letters*, vol. 18, no. 11, pp. 442–444, 1982.